Efficient diffraction control using a tunable active-Raman gain medium

Sandeep Sharma *

Department of Physics, Korea Advanced Institute of Science and Technology (KAIST), Daejeon 34141, South Korea

(Received 16 November 2022; accepted 17 January 2023; published 1 February 2023)

We present a scheme to create an all-optical tunable and lossless waveguide using a controllable coherent Raman process in an atomic rubidium vapor in an $\mathcal{N}$-type configuration. We employ a Gaussian Raman field and a Laguerre-Gaussian control field to imprint a high-contrast tunable waveguidelike feature inside the atomic medium. We numerically demonstrate that such a waveguide is able to guide arbitrary modes of a weak probe beam to several Rayleigh lengths without diffraction and absorption. Our results on an all-optical waveguide-based scheme may have potential applications in lossless image processing, high-contrast biomedical imaging, and image metrology.

DOI: 10.1103/PhysRevA.107.023701

I. INTRODUCTION

Optical diffraction poses a major obstacle in the path of achieving high-contrast imaging, efficient information transfer, and processing. This is because diffraction deforms the optical beam carrying the information, thereby causing a loss of it and thus limiting the efficiency of information processing and imaging methods. To control optical diffraction, different techniques based on coherent quantum effects such as electromagnetically induced transparency [1–3], coherent population trapping [4], double dark resonance [5], and saturated absorption [6] have been proposed. The main idea of these techniques is to make use of the coherent effects and spatially modulate the susceptibility of an atomic medium using a suitable spatially dependent strong field. Such modulation of the susceptibility by a spatially dependent strong field leads to the formation of waveguidelike features inside the atomic medium. This induced waveguide can thus control the diffraction of arbitrary modes of the optical beam propagating through the medium. Apart from diffraction control, such spatially dependent techniques have also been used to study cloning and transfer of images [7–11], generation of structured beams [12–15], vortex beams [16], and in localization of atoms [17].

Moreover, all the abovementioned techniques have been used to create waveguides inside an absorptive medium. Hence, the optical beam carrying information suffers from large absorption while propagating in the induced waveguide. To overcome this problem, similar spatially dependent techniques have been used to create a waveguide inside an active-Raman gain (ARG) medium, which supports lossless propagation of arbitrary modes of the optical beam without diffraction [18,19]. Nonetheless, this waveguide has its own disadvantage, which is inducing high gain in the optical beam propagating through the ARG medium. Such high gain can create instability in the medium [20]. So, to control this high gain, an additional strong control field is applied to the ARG medium [21]. It has been shown that a strong control field significantly reduces gain for the optical beam propagating through the medium. This interesting behavior shown by the control field has been later used to study optical precursors [22], steering and splitting of optical beams [23], and tunable atomic grating [24]. However, in the context of diffraction control, the effect of this control field on the induced waveguide inside the ARG medium has remained unexplored.

In this paper, we investigate the effect of this additional control field on the induced waveguide inside the ARG medium. In this regard, we first start by creating a waveguide inside the medium using a Gaussian Raman beam. We find that the features of the waveguide such as the width of the core and the length of the waveguide can be controlled by the width of the Raman beam. Most importantly, we next use a Laguerre-Gaussian control beam and examine its effect on the properties of the induced waveguide. We find that this control beam induces a waveguide with a very narrow core without changing its length, unlike the earlier case where waveguide length decreases with the narrowing of the core. Waveguides with narrow cores play a very crucial role in controlling the diffraction of optical beams having very narrow feature sizes. Our numerical result on optical beam propagation confirms that this control-beam-induced waveguide can efficiently control diffraction of arbitrary modes of optical beams with feature sizes of $\sim$10 μm to several Rayleigh lengths of the beam, while the waveguide induced by only Raman beam fails in this aspect. Further, controlling the diffraction of optical beams with narrow feature sizes serves an important purpose of achieving high-density information processing and high-contrast imaging. Hence, in this regard, this work is very important and holds a greater advantage over other absorptive/gain-based induced waveguides, as the latter's ability to guide arbitrary modes of optical beams is limited to a feature size of $\sim$50 μm and above [1,4,6,19].

This paper is organized in the following manner: In Sec. II, we propose our model system and present the governing density matrix equations for the system. Next, we provide an analytical expression for the susceptibility of the medium in the steady-state limit and then the beam propagation

*quanta.sandeep@gmail.com

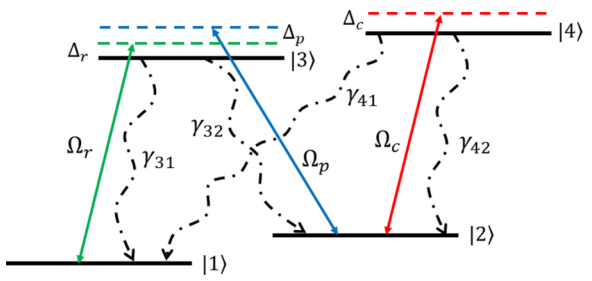

FIG. 1. Displays a schematic diagram of four level $\mathcal{N}$-type atomic system. The transitions $|3\rangle \leftrightarrow |1\rangle$ is coupled by a strong Raman field with Rabi frequency Ω_r. A weak probe field with Rabi frequency Ω_p couples the transition $|3\rangle \leftrightarrow |2\rangle$. The transition $|4\rangle \leftrightarrow |2\rangle$ is driven by a strong control field with Rabi frequency Ω_c. γ_{ij} are the spontaneous decay rates from excited states $|i\rangle$ to ground states $|j\rangle$. The field detunings for Raman, probe, and control are represented as Δ_r, Δ_p, and Δ_c, respectively.

equation in the paraxial limit. In Sec. III, we present our results on the creation of a Raman- and control-field-induced tunable waveguide and on its ability to control diffraction of arbitrary modes of optical beams. Finally, in Sec. IV we conclude our work and suggest its potential application in the field of optics.

II. THEORETICAL FORMALISM

A. Model system

In this work, we consider a tunable ARG system in an $\mathcal{N}$-type configuration as shown in Fig. 1. The proposed configuration can be experimentally realized by considering the energy levels of ^{87}Rb, with the two metastable ground states designated as $|1\rangle = |5S_{\frac{1}{2}}, F = 1\rangle$ and $|2\rangle = |5S_{\frac{1}{2}}, F = 2\rangle$, and the remaining two excited states designated as $|3\rangle = |5P_{\frac{3}{2}}, F' = 1\rangle$ and $|4\rangle = |5P_{\frac{3}{2}}, F' = 2\rangle$. As depicted in Fig. 1, we consider three laser fields acting on the electric-dipole-allowed transitions $|3\rangle \leftrightarrow |1\rangle$, $|3\rangle \leftrightarrow |2\rangle$, and $|4\rangle \leftrightarrow |2\rangle$, thereby forming an $\mathcal{N}$-type configuration. The transition $|3\rangle \leftrightarrow |1\rangle$ is driven by a strong Raman field ($\mathcal{E}_r$) with frequency ω_r, while a weak probe field ($\mathcal{E}_p$) with frequency ω_p couples the transition $|3\rangle \leftrightarrow |2\rangle$. A strong control field ($\mathcal{E}_c$) with frequency ω_c drives the transition $|4\rangle \leftrightarrow |2\rangle$. We define the electric field of all of the three laser fields as

$$\vec{E}_j(\vec{r}, t) = \hat{e}_j \mathcal{E}_j(\vec{r})\, e^{-i(\omega_j t - k_j z)} + \text{c.c.}, \tag{1}$$

where $\hat{e}_j$ is the unit polarization vector, $\mathcal{E}_j(\vec{r})$ is the slowly varying envelope, ω_j is the frequency of the laser field, and k_j is the wave number, respectively. The index $j \in \{r, p, c\}$ indicates the Raman, probe, and control fields, respectively. In the presence of these three laser fields, the time-dependent Hamiltonian of the system under the electric-dipole approximation can be expressed as

$$H = H_0 + H_I, \tag{2a}$$

$$H_0 = \hbar\omega_{12}|2\rangle\langle 2| + \hbar\omega_{13}|3\rangle\langle 3| + \hbar\omega_{14}|4\rangle\langle 4|, \tag{2b}$$

$$H_I = -(|3\rangle\langle 1|\boldsymbol{d}_{31}\cdot\mathcal{E}_r e^{-i(\omega_r t - k_r z)} + |3\rangle\langle 2|\boldsymbol{d}_{32}\cdot\mathcal{E}_p e^{-i(\omega_p t - k_p z)} + |4\rangle\langle 2|\boldsymbol{d}_{42}\cdot\mathcal{E}_c e^{-i(\omega_c t - k_c z)} + \text{H.c.}). \tag{2c}$$

Here $\boldsymbol{d}_{ij} = \langle i|\boldsymbol{d}|j\rangle$ represents the dipole moment of the transition $|i\rangle \leftrightarrow |j\rangle$. To remove the time dependencies from the Hamiltonian in Eq. (2), we make use of the following unitary transformation:

$$W = e^{-\frac{i}{\hbar}Ut}, \tag{3a}$$

$$U = \hbar\omega_r|3\rangle\langle 3| + \hbar(\omega_r - \omega_p)|2\rangle\langle 2| + \hbar(\omega_r - \omega_p + \omega_c)|4\rangle\langle 4|, \tag{3b}$$

and we rewrite the Hamiltonian into a time-independent form under the rotating-wave approximation as

$$\frac{\mathcal{H}_I}{\hbar} = (\Delta_p - \Delta_r)|2\rangle\langle 2| + (\Delta_p - \Delta_r - \Delta_c)|4\rangle\langle 4| - \Delta_r|3\rangle\langle 3| - \Omega_r|3\rangle\langle 1| - \Omega_p|3\rangle\langle 2| - \Omega_c|4\rangle\langle 2| + \text{H.c.}, \tag{4}$$

where $\Delta_r = \omega_r - \omega_{31}$, $\Delta_p = \omega_p - \omega_{32}$, and $\Delta_c = \omega_c - \omega_{42}$ are the detuning of the Raman, probe, and control fields, respectively. The Rabi frequencies of the Raman (Ω_r), probe (Ω_p), and control fields(Ω_c) are defined as

$$\Omega_r = \frac{\vec{d}_{31}\cdot\vec{\mathcal{E}}_{\text{r}}}{\hbar} e^{ik_r z}, \quad \Omega_p = \frac{\vec{d}_{32}\cdot\vec{\mathcal{E}}_{\text{p}}}{\hbar} e^{ik_p z}, \quad \Omega_c = \frac{\vec{d}_{42}\cdot\vec{\mathcal{E}}_{\text{c}}}{\hbar} e^{ik_c z}. \tag{5}$$

To study the effect of the three laser fields on the atomic populations and coherences of the system, we use the following Liouville equation:

$$\frac{\partial\rho}{\partial t} = -\frac{i}{\hbar}[\mathcal{H}_I, \rho] + \mathcal{L}\rho. \tag{6}$$

Here, the last term $\mathcal{L}\rho$ is the Liouvillian operator, which describes the effect of relaxation by radiative decay and is expressed as

$$\mathcal{L}\rho = -\sum_{i=3}^{4}\sum_{j=1}^{2}\frac{\gamma_{ij}}{2}(|i\rangle\langle i|\rho - 2|j\rangle\langle j|\rho_{ii} + \rho|i\rangle\langle i|), \tag{7}$$

where γ_{ij} corresponds to radiative decay rates from excited states $|i\rangle$ to ground states $|j\rangle$. Next, by incorporating Eqs. (4) and (7) in Eq. (6), we can write the equation for density matrix elements corresponding to the atomic populations and coherences of the system as

$$\dot{\rho}_{11} = \gamma_{31}\rho_{33} + \gamma_{41}\rho_{44} + i\Omega_r^*\rho_{31} - i\Omega_r\rho_{13}, \tag{8a}$$

$$\dot{\rho}_{22} = \gamma_{32}\rho_{33} + \gamma_{42}\rho_{44} + i\Omega_p^*\rho_{32} - i\Omega_p\rho_{23} + i\Omega_c^*\rho_{42} - i\Omega_c\rho_{24}, \tag{8b}$$

$$\dot{\rho}_{33} = -(\gamma_{31} + \gamma_{32})\rho_{33} + i\Omega_r\rho_{13} - i\Omega_r^*\rho_{31} + i\Omega_p\rho_{23} - i\Omega_p^*\rho_{32}, \tag{8c}$$

$$\dot{\rho}_{21} = -[\gamma_c + i(\Delta_p - \Delta_r)]\rho_{21} - i\Omega_r\rho_{23} + i\Omega_p^*\rho_{31} + i\Omega_c^*\rho_{41}, \tag{8d}$$

$$\dot{\rho}_{31} = -\left[\frac{\gamma_{31} + \gamma_{32}}{2} - i\Delta_r\right]\rho_{31} + i\Omega_p\rho_{21} + i\Omega_r(\rho_{11} - \rho_{33}), \tag{8e}$$

$$\dot{\rho}_{32} = -\left[\frac{\gamma_{31} + \gamma_{32}}{2} - i\Delta_p\right]\rho_{32} + i\Omega_r\rho_{12} - i\Omega_c\rho_{34} + i\Omega_p(\rho_{22} - \rho_{33}), \tag{8f}$$

$$\dot{\rho}_{34} = -\left[\frac{\gamma_{31}+\gamma_{32}+\gamma_{41}+\gamma_{42}}{2} - i(\Delta_p - \Delta_c)\right]\rho_{34} + i\Omega_r\rho_{14} + i\Omega_p\rho_{24} - i\Omega_c^*\rho_{32}, \tag{8g}$$

$$\dot{\rho}_{41} = -\left[\frac{\gamma_{41}+\gamma_{42}}{2} + i(\Delta_p - \Delta_r - \Delta_c)\right]\rho_{41} + i\Omega_c\rho_{21} - i\Omega_r\rho_{43}, \tag{8h}$$

$$\dot{\rho}_{42} = -\left[\frac{\gamma_{41}+\gamma_{42}}{2} - i\Delta_c\right]\rho_{42} - i\Omega_p\rho_{43} + i\Omega_c(\rho_{22} - \rho_{44}), \tag{8i}$$

where the time derivatives are denoted by overdots and the complex conjugates are denoted by "*". The remaining equations for the density matrix elements can be found from the property of conjugate $\dot{\rho}_{ji}^* = \dot{\rho}_{ij}$ and the population conservation condition $\sum_{i=1}^{4}\rho_{ii} = 1$.

B. Expression for linear susceptibility

In this section, we provide an analytical expression for the linear susceptibility of the system derived in the steady-state limit using a perturbative method. In this method, we assume almost all the atoms to be in state $|1\rangle$, i.e., $\rho_{11} \approx 1$. Now, as a strong Raman field is applied to the $|1\rangle \leftrightarrow |3\rangle$ transition, the condition for atoms to remain in state $|1\rangle$ is made possible by considering the Raman field to be highly detuned from excited state $|3\rangle$. In addition to this, we also consider the weak probe field, which connects the adjacent transition $|3\rangle \leftrightarrow |2\rangle$ to be highly detuned. This arrangement of both the fields turns the system into an active-Raman gain system where the probe sees Raman gain around the two-photon resonance condition [21]. Apart from this, we also apply a strong control field to modulate this induced Raman gain in the probe field. Further, it is necessary to mention here that the detuning of this control field has a very negligible effect on the population in state $|1\rangle$. So, for this configuration, we expand the density matrix to first order in the probe as it is considered weak, and we keep only up to the second-order terms corresponding to the Raman field as the Raman process is a second-order process [23]. With these assumptions, the density matrix is then expanded in the following manner:

$$\rho_{ij} = \rho_{ij}^{(0)} + \frac{\Omega_r}{\gamma}\rho_{ij}^{(1)} + \frac{\Omega_r^*}{\gamma}\rho_{ij}^{(2)} + \frac{\Omega_p}{\gamma}\rho_{ij}^{(3)} + \frac{\Omega_p^*}{\gamma}\rho_{ij}^{(4)} + \frac{\Omega_r^2}{\gamma^2}\rho_{ij}^{(5)} + \frac{|\Omega_r|^2}{\gamma^2}\rho_{ij}^{(6)} + \frac{\Omega_r^{*2}}{\gamma^2}\rho_{ij}^{(7)} + \frac{\Omega_r\Omega_p}{\gamma^2}\rho_{ij}^{(8)} + \frac{\Omega_r^*\Omega_p}{\gamma^2}\rho_{ij}^{(9)} + \frac{\Omega_r\Omega_p^*}{\gamma^2}\rho_{ij}^{(10)} + \frac{\Omega_r^*\Omega_p^*}{\gamma^2}\rho_{ij}^{(11)} + \frac{\Omega_p|\Omega_r|^2}{\gamma^3}\rho_{ij}^{(12)}. \tag{9}$$

Here γ represents the total spontaneous decay rate of excited states $|3\rangle$ and $|4\rangle$. Further, $\rho_{ij}^{(0)}$ is the zeroth-order solution determined in the absence of all fields, and $\rho_{ij}^{(k)}$ with $k \in \{1-12\}$ is the kth-order solution of the density matrix equation. We now substitute the above equation in Eq. (8) and equate the coefficients of zeroth order and each of the kth-order terms. As a result, we obtain a total of 13 different sets of coupled density matrix equations corresponding to each of the $\rho_{ij}^{(k)}$ and $\rho_{ij}^{(0)}$ terms. Next, we solve these 13 different sets of equations for $\rho_{ij}^{(k)}$ and $\rho_{ij}^{(0)}$ in the steady-state limit and substitute their expression in Eq. (9) to obtain the full expression of the atomic populations and coherences ρ_{ij}. In this work, we are interested in studying the effect of the medium on the probe field, so we focus on the atomic coherence ρ_{32} which yields the linear response of the medium. We then write this linear response (susceptibility) χ_p of the medium at probe frequency ω_p in terms of the atomic coherence ρ_{32} as

$$\chi_p(\omega_p) = \frac{\mathcal{N}|d_{32}|^2}{\hbar\Omega_p}\rho_{32},$$

$$\rho_{32} = \frac{-i\,\Omega_p|\Omega_r|^2}{(\gamma_{32} - i\Delta_p)\,\Gamma_a + |\Omega_c|^2}\left[\frac{\Gamma_a}{\left(\frac{\gamma_{31}+\gamma_{32}}{2}\right)^2 + \Delta_r^2} + A\right],$$

$$A = \frac{\Gamma_a\Gamma_b - |\Omega_c|^2}{\left[\left(\frac{\gamma_{31}+\gamma_{32}}{2}\right) + i\Delta_r\right][\Gamma_b\Gamma_c + |\Omega_c|^2]}, \tag{10}$$

where $\Gamma_a = \frac{(\gamma_{31}+\gamma_{32}+\gamma_{41}+\gamma_{42})}{2} - i(\Delta_p - \Delta_c)$, $\Gamma_b = \frac{(\gamma_{41}+\gamma_{42})}{2} + i(\Delta_r - \Delta_p + \Delta_c)$, and $\Gamma_c = \gamma_c + i(\Delta_r - \Delta_p)$. The susceptibility expression in Eq. (10) clearly depicts its dependence on both Raman and control field intensities. Hence, by suitably manipulating both these fields, we can control the susceptibility of the medium and ultimately control the propagation dynamics of the probe field. In the following section, we present the equation which shows how this susceptibility regulates the propagation of the probe beam traveling through the atomic medium.

C. Propagation equation

In order to study the propagation of the probe field through the atomic medium, we use Maxwell's wave equation under the slowly varying envelope and paraxial-wave approximation and write it in terms of the Rabi frequency of the probe field in the following form:

$$\frac{\partial}{\partial z}\Omega_p = \frac{i}{2k_p}\left(\frac{\partial^2}{\partial x^2} + \frac{\partial^2}{\partial y^2}\right)\Omega_p + 2i\pi k_p\chi_p\,\Omega_p. \tag{11}$$

The first terms on the right-hand side of Eq. (11) lead to diffraction of the probe beam propagating either in free space or through any medium. The second term on the right-hand side of Eq. (11) represents the effect of the medium on the propagation of the probe beam. It is interesting to notice from Eq. (11) that, if we suitably modulate the medium susceptibility in the transverse direction, then we can eventually overcome the effect of diffraction. In the next section, we discuss on the manipulation of the medium susceptibility in the transverse direction and its effect on the probe beam propagation.

III. NUMERICAL RESULTS AND DISCUSSION

A. Homogeneous linear susceptibility

In this subsection, we first analyze the effect of continuous-wave (cw) Raman and control fields on the medium susceptibility. In this regard, we numerically evaluate the medium

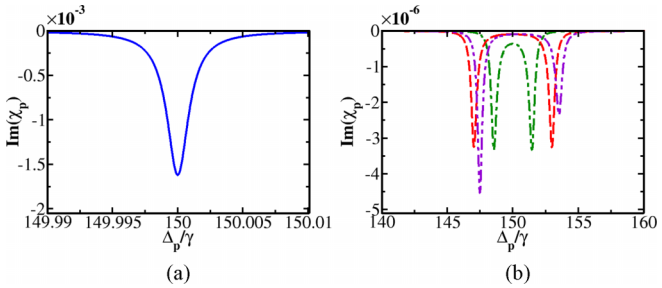

FIG. 2. Variation of the imaginary part of susceptibility with probe detuning, in the absence of the control field (a) and in presence of the control field (b). The parameters for panel (a) are $\Omega_r^0 = 2\gamma$, $\Omega_c^0 = 0\gamma$, and $\Delta_c = 0\gamma$. The parameters for panel (b) are $\Omega_r^0 = 2\gamma$, $\Omega_c^0 = 1.5\gamma$, and $\Delta_c = 0\gamma$ (green dotted-dashed line); $\Omega_r^0 = 2\gamma$, $\Omega_c^0 = 3.0\gamma$, and $\Delta_c = 0\gamma$ (red-dashed line); $\Omega_r^0 = 2\gamma$, $\Omega_c^0 = 3.0\gamma$, and $\Delta_c = 10\gamma$ (violet double dotted-dashed line). Other parameters are $\gamma_{31} = 0.5\gamma$, $\gamma_{32} = 0.5\gamma$, $\gamma_{41} = 0.5\gamma$, $\gamma_{42} = 0.5\gamma$, $\gamma_c = 10^{-3}\gamma$, $\Delta_r = 150\gamma$, $\lambda = 795$ nm, and $\mathcal{N} = 3 \times 10^{12}$ atoms/cm^3.

susceptibility as in Eq. (10), first in presence of only the cw Raman field and then in presence of both the cw Raman field and the cw control field. The result of our simulation is presented in Fig. 2, where the plot shows the variation of imaginary parts of susceptibility with probe detuning. In Fig. 2(a), it can be seen that in presence of a Raman field the probe sees a Raman gain around the two-photon resonance condition $\Delta_p - \Delta_r = 0$. This is due to the fact that a strong Raman field acts between the levels $|3\rangle$ and $|1\rangle$ that has a population in a lower state and thus induces gain for the weak probe field which acts on the unpopulated levels $|3\rangle \leftrightarrow |2\rangle$, under the highly detuned condition [21,25]. A detailed theoretical analysis of this Raman gain process can be found in Refs. [26,27]. Next, when a strong control field is applied to the $|4\rangle \leftrightarrow |2\rangle$ transition, then the probe sees a significant reduction in gain at the two-photon resonance condition because of the splitting of the single Raman gain peak into two, as shown in Fig. 2(b). This splitting can be attributed to the fact that a strong control field dresses the levels $|4\rangle$ and $|2\rangle$ into the superposition states $|\pm\rangle = (|4\rangle \pm |2\rangle)/\sqrt{2}$. As a result, the probe sees two Raman gain peaks corresponding to the transitions $|3\rangle \leftrightarrow |+\rangle$ and $|3\rangle \leftrightarrow |-\rangle$, respectively [28]. Further, the splitting between the two Raman gain peaks is proportional to Ω_c. With the increase in Ω_c, the splitting between the gain peaks increases and the Raman gain around two-photon resonance decreases, as can be seen in Fig. 2(b). Moreover, from Fig. 2(b), it can be seen that the gain peaks become asymmetric when the control field is slightly off-resonant. This is because when the control field is off-resonant the energy splitting between $|+\rangle$ and $|-\rangle$ becomes asymmetric, i.e, the energy of state $|-\rangle$ comes closer to the resonant value and that of $|+\rangle$ moves away from the resonant value [28]. As a result, state $|-\rangle$ sees a larger gain than state $|+\rangle$ as depicted in Fig. 2(b). From the above discussion, it is evident that a strong control field plays an important role in controlling the Raman gain seen by the probe. So, in the next section, we discuss how this Raman gain modulation by the strong control field can be a major factor in the creation of a tunable waveguidelike structure inside the atomic medium.

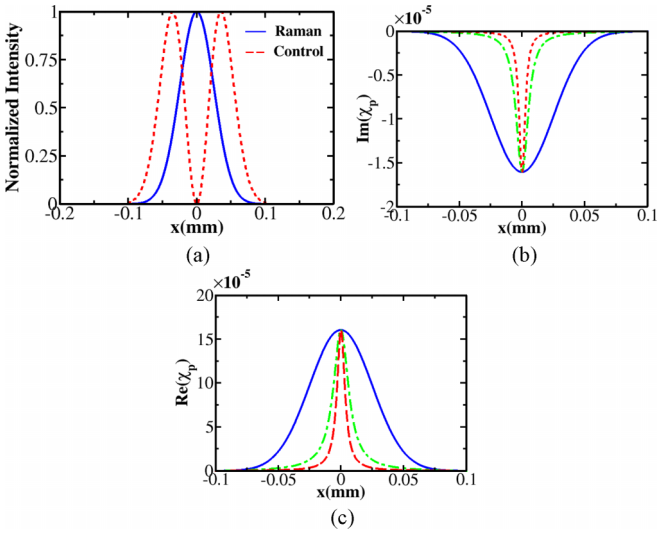

FIG. 3. Panel (a) displays the spatial variation of Raman and control beam profiles in the x direction at the $y = 0$ plane. Panels (b) and (c) show the variation of the imaginary and real parts of susceptibility in the x direction at the $y = 0$ plane, respectively, in the absence (blue solid line) and in the presence (red dashed and green dotted-dashed lines) of the control field. The parameters for the blue solid line are $\Omega_r^0 = 2\gamma$ and $\Omega_c^0 = 0\gamma$, for the green dotted-dashed line they are $\Omega_r^0 = 2\gamma$ and $\Omega_c^0 = 1.5\gamma$, and for the red-dashed line they are $\Omega_r^0 = 2\gamma$ and $\Omega_c^0 = 3\gamma$. In addition to $w_r = 50$ μm, $w_c = 50$ μm, and $\Delta_p = 150.01\gamma$, all other parameters are same as those in Fig. 2 except for $\Delta_c = 10\gamma$.

B. Inhomogeneous linear susceptibility

In this subsection, we investigate the effect of spatially dependent Raman and control fields on the susceptibility of the atomic medium. For this, we consider the Raman field as a Gaussian beam and the control field as a Laguerre-Gaussian (LG) beam. The spatial profiles of both beams are expressed as

$$\Omega_r(x,y,z) = \Omega_r^0 \frac{w_{0r}}{w_r(z)} e^{-\left(\frac{r^2}{w_r^2(z)}\right)} e^{\left(\frac{ikr^2}{2R_r(z)}\right)} e^{[kz - i\tan^{-1}\left(\frac{z}{z_{0r}}\right)]}, \quad (12a)$$

$$\Omega_c(x,y,z) = \Omega_c^0 \frac{w_{0c}}{w_c(z)} \left(\frac{r\sqrt{2}}{w_c(z)}\right) e^{-\left(\frac{r^2}{w_c^2(z)}\right)} e^{\left(\frac{ikr^2}{2R_c(z)}\right)} \times e^{i[\phi - 2\tan^{-1}\left(\frac{z}{z_{0c}}\right)]}, \quad (12b)$$

where $r = \sqrt{x^2 + y^2}$ and $\phi = \tan^{-1}(\frac{y}{x})$. Also, $w_j(z) = w_{0j}\sqrt{1 + [(z-q)/z_{0j}]^2}$ and $R_j(z) = z + (z_{0j}^2/z)$ are the spot size and radius of curvature of the beams, respectively, with w_{0j} being the minimum beam waist at focusing point q and $z_{0j} = \pi w_{0j}^2/\lambda$ being the Rayleigh length of the beams. The index $j \in \{r, c\}$, which represents the Raman and control beams, respectively.

Initially, we consider the case when only the Raman beam is present and thus examine the behavior of the susceptibility in the transverse direction using Eq. (10). We present the results of our simulation in Fig. 3. Figure 3(b) shows that, in the presence of a Gaussian Raman beam [see Fig. 3(a) for spatial profile], the probe beam sees a spatial gain profile in the transverse direction x at the $y = 0$ plane. This can be

explained using the fact that the Raman beam induces a gain in the probe beam as explained in Sec. III A, also shown in Fig. 2(a). Hence, the probe beam will see gain only at the spatial position where the Raman beam is present, leading to the formation of a gain window in the transverse direction similar to the profile of the Raman beam. Interestingly, when the probe is slightly blue-detuned from the two-photon resonance, it sees a waveguidelike feature inside the medium as shown in Fig. 3(c). The variation of the refractive index in the transverse direction as shown in Fig. 3(c) depicts a variation similar to the waveguide where the central region has an index (core) higher than that of the regions away from the center (cladding). Further, it can be seen in Fig. 3(c) that the refractive index profile also has a similar spatial shape in the transverse direction like the Raman Gaussian beam. As a result of this spatial similarity, the width of the core region can be considered to be equal to the width of the Raman beam, i.e., $w_r(z)$. Accordingly, the length of the waveguide can then be attributed to being equivalent to the Rayleigh length $z_{0r} = \pi w_{0r}^2/\lambda$ of the Raman beam. Within this length, the width of the Raman beam does not change much and hence the properties of the induced waveguide remain intact. So, from the above discussion, it is apparent that a spatially dependent Raman beam plays a major role in creating a waveguidelike feature inside the medium, which in turn can be able to support diffractionless propagation of optical beams [18,19].

Nevertheless, in the next section, we show that this Raman-induced optical waveguide (RIW) is unable to control efficiently the diffraction of narrow optical beams. To control the diffraction of narrow optical beams, a high-contrast waveguide with a narrow core region is required. For the case of the RIW, a high-contrast waveguide with a narrow core region can be achieved by increasing the atomic density of the system as well as by narrowing the width $w_r(z)$ of the Raman beam. This configuration, however, increases gain significantly and also reduces the length of the waveguide (z_{0r}), making it less efficient for diffraction control.

To overcome this problem, we make use of an additional spatial-dependent control beam that can control the features of the waveguide. In this regard, we consider the control beam to be a LG beam as shown in Fig. 3(a). This particular spatial profile of the control beam creates a very narrow gain profile as well as a waveguide with a very narrow core region, which is shown in Figs. 3(b) and 3(c), respectively. Such spatial modulation in the gain as well as the refractive index of the medium can be attributed to the fact that the presence of a control beam decreases gain in the system, as explained in Sec. III A. Now, since the intensity distribution for the LG beam is a doughnut shape with zero intensity at the center and maximum intensity in the annular region, the spatial gain will be reduced in this annular region, resulting in the narrowing of the spatial gain profile. A similar reduction in the refractive index in the annular region is noticed due to the presence of the LG control beam, which leads to the creation of a waveguide with a narrow core. Also, from Figs. 3(b) and 3(c), it can be seen that, with the increase in control field strength, the gain window and the core of the waveguide become narrow. This again can be related to the fact that, with an increase in control field strength, gain decreases and so does the refractive

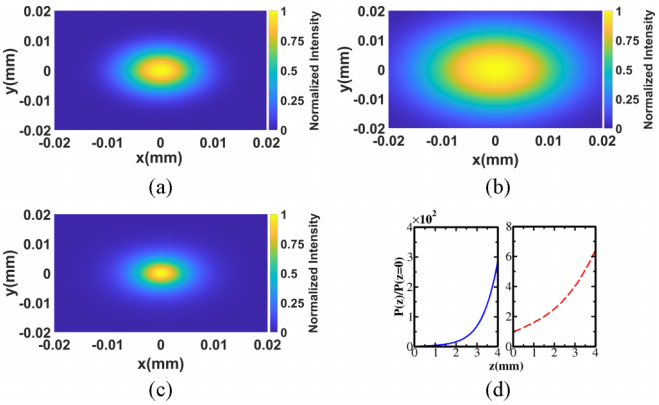

FIG. 4. Panel (a) shows the normalized intensity of the input probe beam (HG_{00}) in the transverse x-y plane. Panels (b) and (c) show the output intensity of the probe beam in the absence of the control beam and in the presence of the control beam, respectively, at a propagation distance of $z = 4$ mm. Panel (d) shows the evolution of the integrated power of the probe beam in the absence of the control beam (blue solid line) and in the presence of the control beam (red dashed line), with the propagation distance z. The parameters are $\Omega_p^0 = 0.001\gamma$, $w_p = 10$ μm, $\Omega_r^0 = 2\gamma$, $\Omega_c^0 = 3.5\gamma$, and $q_1 = q_2 = 2$. Other parameters are the same as those in Fig. 3.

index as explained in Sec. III A. Moreover, it is interesting to note that, unlike the RIW case where the waveguide narrowing is only possible by narrowing the width of the Raman beam, which leads to a decrease in waveguide length, here the narrowing of the waveguide is mainly due to the spatial shape of the control beam, which leaves the waveguide length unchanged. Hence, the spatial profile of the control beam plays a decisive role in controlling the features of the waveguide and in creating a high-contrast tunable waveguide in the medium. In the following subsection, we show how this control beam tunable Raman-induced waveguide (CRIW) holds a greater advantage over the RIW in controlling the diffraction of narrow optical beams.

C. Probe beam propagation

In this subsection, we explore the possibility of diffractionless propagation of arbitrary modes of narrow optical beams in the RIW and the CRIW created inside the atomic medium. For this, we consider the initial profile of the probe beam as different Hermite-Gaussian modes, which are expressed as

$$\Omega_p(x, y, z = 0) = \Omega_p^0 H_n\left(\frac{\sqrt{2}x}{w_p}\right) H_m\left(\frac{\sqrt{2}y}{w_p}\right) e^{-\frac{(x^2+y^2)^2}{w_p^2}}, \tag{13}$$

where H_n and H_m are the Hermite polynomials of orders n and m, respectively. With the abovementioned different initial profile, we study the propagation of the probe beam by numerically solving Eq. (11) using the Fourier split-step method [29]. We first consider the propagation of the HG_{00} (Gaussian) probe beam with a width (w_p) of 10 μm in the RIW and present the results of our simulation in Fig. 4. Figure 4(b) shows the intensity distribution of the output probe

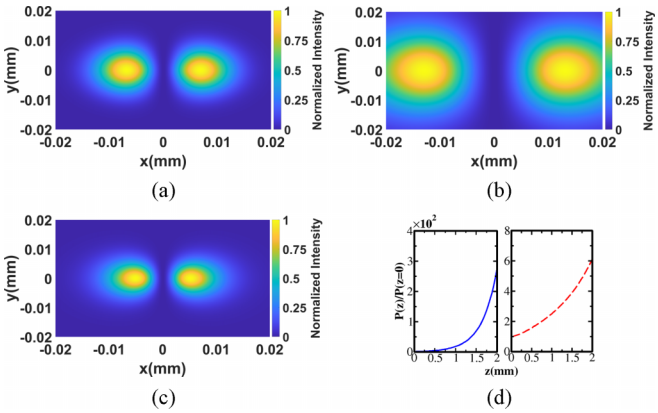

FIG. 5. Panel (a) shows the normalized intensity of the input probe beam (HG_{10}) in the transverse x-y plane. Panels (b) and (c) show the output intensity of the probe beam in the absence of the control beam and in the presence of the control beam, respectively, at a propagation distance of $z = 2$ mm. Panel (d) shows the evolution of integrated power of the probe beam in the absence of the control beam (blue solid line) and in presence of the control beam (red dashed line), with the propagation distance z. All parameters are same as those in Fig. 4 except for $\Omega_c^0 = 3\gamma$, $w_r = 60$ μm, $w_c = 60$ μm, and $\mathcal{N} = 8 \times 10^{12}$ atoms/cm^3.

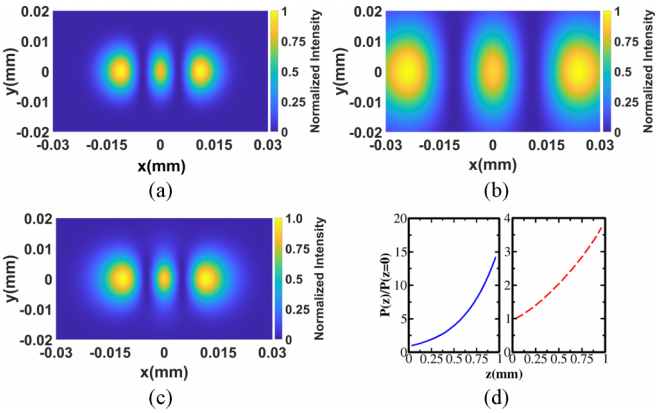

FIG. 6. Panel (a) shows the normalized intensity of the input probe beam (HG_{20}) in the transverse x-y plane. The output intensity of the probe beam, shown in the absence of the control beam (b) and in the presence of the control beam (c), at a propagation distance of $z = 1$ mm. Panel (d) shows the variation of integrated power of the probe beam with the propagation distance z, in the absence of the control beam (blue solid line) and in the presence of the control beam (red dashed line). The parameters are $\Omega_c^0 = 3\gamma$, $w_r = 90$ μm, $w_c = 90$ μm, $\Delta_r = 195\gamma$, $\Delta_c = 55\gamma$, $\Delta_p = 195.01\gamma$, and $\mathcal{N} = 1 \times 10^{13}$ atoms/cm^3. Other parameters are the same as those in Fig. 4.

beam in the transverse plane after propagating a distance of $z = 4$ mm in the RIW. It is clear from Fig. 4(b) that the probe beam gets diffracted after propagating through this induced waveguide. This is because the RIW has a wide core and is unable to control the diffraction of the probe beam. In addition to this, we also study the output probe power $P(z) = \iint |\Omega_p(x, y, z)|^2 dx\, dy$ and find that the probe beam is highly amplified by a factor of 100 after propagating a distance of $z = 4$ mm, as shown in Fig. 4(d). So, due to its inability to control diffraction along with the creation of such a large gain in the probe beam, which can lead to instability in the medium [20], the practical applicability of the RIW is severely limited.

However, this problem is eventually overcome by utilizing an additional LG control beam, which can efficiently control both diffraction as well as gain in the probe beam, as shown in Figs. 4(c) and 4(d), respectively. Such control over diffraction by the control beam can be attributed to the creation of a waveguide with a narrow core, which is explained in detail in Sec. III B. In addition to diffraction control, the probe beam is also slightly focused as shown in Fig. 4(c). Such focusing behavior has been observed earlier in atomic-based waveguides [19] and can be controlled by suitably modulating the features of the waveguide. Further, it is interesting to notice that the probe beam propagates without diffraction in this narrow waveguide [see Fig. 4(c)] up to a distance of 4 mm, which is 10 times the Rayleigh length of the probe beam z_{0p}. Also, unlike in earlier cases, here the probe beam attains a reasonable amount of gain at a distance of 4 mm, as shown in Fig. 4(d). Our result on diffraction control of narrow optical beams to several Rayleigh lengths may have potential application in high-density lossless information transfer to macroscopic lengths and high-contrast imaging.

Further, in this work, we are dealing with the propagation of optical beams in a waveguide induced inside a gain system. So, it is necessary to verify the validity of both the weak-field approximation and the paraxial approximation used in the calculation. In this regard, for our numerical calculations on beam propagation, we start with low probe power, and throughout the propagation we find that the maximum intensity of the probe is always very much smaller than the maximum intensity of the Raman and control beams. This condition of probe intensity validates our weak-field approximation. Also, the width of the probe beam w_p does not change much throughout its propagation, and the condition for paraxiality, $\lambda/2\pi w_p < 0.1$, is always satisfied [30], thus validating our paraxial approximation.

Next, to establish that the CRIW can support arbitrary modes of the probe beam, we also study the propagation of HG_{10} and HG_{20} probe beams in it and present our results in Figs. 5 and 6, respectively. From both Figs. 5 and 6, it is noticeable that the CRIW is able to control the diffraction of the probe beam to a length of $5z_{0p}$ and $2.5z_{0p}$, respectively, with a reasonable amount of gain, while the RIW fails to do so. Apart from this, we also performed numerical simulations on the propagation of other higher-order modes of the probe beam and found diffractionless propagation of such modes in the CRIW. Hence, from the above discussions, it becomes evident that the control beam plays an important role in the creation of the CRIW and subsequently in controlling the diffraction of arbitrary modes of narrow optical beams to several Rayleigh lengths.

IV. CONCLUSION

In conclusion, we have investigated diffraction control of arbitrary modes of an optical beam using tunable Raman

effects arising in an atomic medium in an $\mathcal{N}$-type configuration. We have demonstrated that by using a suitable spatially dependent Raman field, a waveguidelike feature can be created inside the atomic medium. Further, we show that the properties of the induced waveguide can be modulated by using an additional spatially dependent control field. From our numerical results on optical beam propagation, we conclude that the RIW is incapable of controlling the diffraction of narrow optical beams, while the CRIW can efficiently control the diffraction of such beams to several Rayleigh lengths. Our results may have a possible application in high-contrast imaging [31,32], information processing [33,34], and lithography [35].

ACKNOWLEDGMENT

We wish to acknowledge the financial support from KAIST through the BK21 Postdoctoral Fellowship.

APPENDIX

1. Perturbative solution

In this Appendix, we provide the solution for the necessary atomic population and coherences evaluated analytically using the perturbative analysis as in Eq. (9). For the Raman process, the values for atomic populations and coherences are given as

$$\rho_{11} = 1, \tag{A1a}$$

$$\rho_{31} = \frac{i\Omega_r}{\left[\frac{\gamma_{31}+\gamma_{32}}{2} - i\Delta_r\right]}, \tag{A1b}$$

$$\rho_{22} = 0, \tag{A1c}$$

$$\rho_{42} = 0. \tag{A1d}$$

From the above solutions, it is evident that most of the population remains in state $|1\rangle$. This is because the Raman field is highly detuned from excited state $|3\rangle$ and hence almost no population is transferred to it and other states [23,26,28]. Also, since the probe field is very weak and highly detuned, there is no effect of the Raman beam on the control beam and vice versa, which is clear from the above coherence expressions ρ_{31} and ρ_{42}.

2. Medium response on Raman beam

Now, as most of the population is in state $|1\rangle$, the medium response on the Raman field is evident from the coherence ρ_{31},

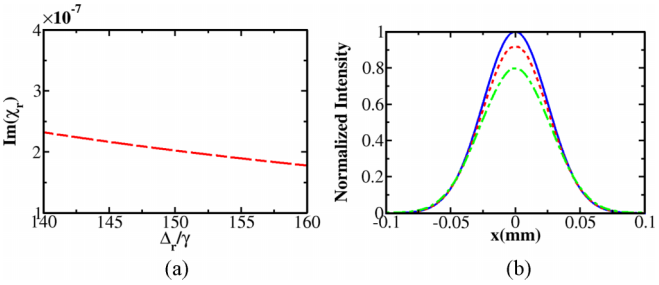

FIG. 7. Panel (a) shows the variation of the imaginary part of susceptibility for the Raman field with Raman detuning. Panel (b) shows the intensity (normalized with initial peak value) of the Gaussian Raman beam at different propagation lengths inside the medium. In panel (b), the blue solid line represents the intensity profile for the input Raman Gaussian beam, the red dashed line represents the intensity of the output Raman beam at $z = 2$ mm, and the green dotted-dashed line represenst the intensity of the output Raman beam at $z = 4$ mm. The parameters considered here are the same as those in Fig. 4.

which corresponds to that of a two-level system. The medium susceptibility of the Raman field can then be expressed as

$$\chi_r(\omega_r) = \frac{\mathcal{N}|d_{31}|^2}{\hbar\Omega_r}\rho_{31}. \tag{A2}$$

We numerically evaluate the above susceptibility and present the result in Fig. 7(a). It is clear from Fig. 7(a) that the medium response on the Raman beam is very weak because of the highly detuned condition. Even though the effect of medium susceptibility on the Raman field is weak, it is necessary to check its effect on the propagation of the Raman beam as it can directly impact the propagation of the probe beam. The effect of medium susceptibility on the Raman beam propagation is governed by the following equation:

$$\frac{\partial}{\partial z}\Omega_r = \frac{i}{2k_r}\left(\frac{\partial^2}{\partial x^2} + \frac{\partial^2}{\partial y^2}\right)\Omega_r + 2i\pi k_r \chi_r \Omega_r. \tag{A3}$$

We numerically solve the above equation by using the Fourier split-step method [29], the result of which is shown in Fig. 7(b). From Fig. 7(b), it is evident that the Raman beam is slightly absorbed after propagating a distance of $z = 4$ mm through the medium. This effect of reduction in Raman beam intensity is taken into consideration while evaluating Fig. 4. However, while evaluating Figs. 5 and 6, we neglect the effect of the medium on the Raman beam as in these figures the propagation length is smaller than that in the earlier case and we found that the medium has a negligible effect on the Raman beam for smaller propagation length.

[1] A. G. Truscott, M. E. J. Friese, N. R. Heckenberg, and H. Rubinsztein-Dunlop, Optically Written Waveguide in an Atomic Vapor, Phys. Rev. Lett. **82**, 1438 (1999).

[2] R. Kapoor and G. S. Agarwal, Theory of electromagnetically induced waveguides, Phys. Rev. A **61**, 053818 (2000).

[3] O. Firstenberg, M. Shuker, N. Davidson, and A. Ron, Elimination of the Diffraction of Arbitrary Images Imprinted on Slow Light, Phys. Rev. Lett. **102**, 043601 (2009).

[4] H. Shpaisman, A. D. Wilson-Gordon, and H. Friedmann, Electromagnetically induced waveguiding in double-Λ systems, Phys. Rev. A **71**, 043812 (2005).

[5] S. Sharma and T. N. Dey, Kerr-field-induced tunable optical atomic waveguide, Phys. Rev. A **96**, 053813 (2017).

[6] T. N. Dey and G. S. Agarwal, Subdiffraction propagation of images using saturated absorption of optical transition, Opt. Lett. **34**, 3199 (2009).

[7] O. N. Verma, L. Zhang, J. Evers, and T. N. Dey, Optical cloning of arbitrary images beyond the diffraction limits, Phys. Rev. A **88**, 013810 (2013).
[8] D.-S. Ding, Z.-Y. Zhou, and B.-S. Shi, Image cloning beyond diffraction based on coherent population trapping in a hot rubidium vapor, Opt. Lett. **39**, 240 (2014).
[9] M. Cao, L. Zhang, Y. Yu, F. Ye, D. Wei, W. Guo, S. Zhang, H. Gao, and F. Li, Transfer and conversion of images based on EIT in atomic vapor, Opt. Lett. **39**, 2723 (2014).
[10] L. Qin, C. Hang, and G. Huang, High-fidelity and controllable cloning of high-dimensional optical beams with a Rydberg atomic gas, Phys. Rev. A **102**, 063707 (2020).
[11] Z. Shi and G. Huang, Selection and cloning of periodic optical patterns with a cold Rydberg atomic gas, Opt. Lett. **46**, 5344 (2021).
[12] N. Radwell, T. W. Clark, B. Piccirillo, S. M. Barnett, and S. Franke-Arnold, Spatially Dependent Electromagnetically Induced Transparency, Phys. Rev. Lett. **114**, 123603 (2015).
[13] S. Sharma and T. N. Dey, Phase-induced transparency-mediated structured-beam generation in a closed-loop tripod configuration, Phys. Rev. A **96**, 033811 (2017).
[14] H. R. Hamedi, J. Ruseckas, E. Paspalakis, and G. Juzeliunas, Transfer of optical vortices in coherently prepared media, Phys. Rev. A **99**, 033812 (2019).
[15] S. Sharma and T. N. Dey, Controlled light shaping via phase-dependent electromagnetically induced transparency, J. Opt. Soc. Am. B **36**, 960 (2019).
[16] H. R. Hamedi, J. Ruseckas, E. Paspalakis, and G. Juzeliunas, Off-axis optical vortices using double-Raman singlet and doublet light-matter schemes, Phys. Rev. A **101**, 063828 (2020).
[17] H. R. Hamedi, V. Kudriasov, N. Jia, J. Qian, and G. Juzeliunas, Ferris wheel patterning of Rydberg atoms using electromagnetically induced transparency with optical vortex fields, Opt. Lett. **46**, 4204 (2021).
[18] P. K. Vudyasetu, D. J. Starling, and J. C. Howell, All Optical Waveguiding in a Coherent Atomic Rubidium Vapor, Phys. Rev. Lett. **102**, 123602 (2009).
[19] T. N. Dey and J. Evers, Nondiffracting optical beams in a three-level Raman system, Phys. Rev. A **84**, 043842 (2011).
[20] G. P. Agrawal, Transverse modulation instability of copropagating optical beams in nonlinear Kerr media, J. Opt. Soc. Am. B **7**, 1072 (1990).
[21] G. S. Agarwal and S. Dasgupta, Superluminal propagation via coherent manipulation of the Raman gain process, Phys. Rev. A **70**, 023802 (2004).
[22] Y. Peng, Y. Niu, L. Zhang, A. Yang, L. Jiang, and S. Gong, Enhanced optical precursors by Doppler effect via active Raman gain process, Opt. Lett. **37**, 3333 (2012).
[23] O. N. Verma and T. N. Dey, Steering, splitting, and cloning of an optical beam in a coherently driven Raman gain system, Phys. Rev. A **91**, 013820 (2015).
[24] V. G. Arkhipkin and S. A. Myslivets, One- and two-dimensional Raman-induced diffraction gratings in atomic media, Phys. Rev. A **98**, 013838 (2018).
[25] L. J. Wang, A. Kuzmich, and A. Dogariu, Gain-assisted superluminal light propagation, Nature (London) **406**, 277 (2000).
[26] Y. Wu, Effective Raman theory for a three-level atom in the Λ configuration, Phys. Rev. A **54**, 1586 (1996).
[27] M. G. Payne and L. Deng, Extremely slow propagation of a light pulse in an ultracold atomic vapor: A Raman scheme without electromagnetically induced transparency, Phys. Rev. A **64**, 031802(R) (2001).
[28] L.-D. Zhang, Y. Jiang, R.-G. Wan, S.-C. Tian, B. Zhang, X.-J. Zhang, J.-Y. Gao, Y.-P. Niu, and S.-Q. Gong, Extremely narrowed and amplified gain spectrum induced by the Doppler effect, J. Phys. B: At. Mol. Opt. Phys. **44**, 135505 (2011).
[29] A. D. Bandrauk and H. Shen, High-order split-step exponential methods for solving coupled nonlinear Schrodinger equations, J. Phys. A: Math. Gen. **27**, 7147 (1994).
[30] G. P. Agrawal and D. N. Pattanayak, Gaussian beam propagation beyond the paraxial approximation, J. Opt. Soc. Am. **69**, 575 (1979).
[31] K. T. Kapale and G. S. Agarwal, Subnanoscale resolution for microscopy via coherent population trapping, Opt. Lett. **35**, 2792 (2010).
[32] H. Li, V. A. Sautenkov, M. M. Kash, A. V. Sokolov, G. R. Welch, Y. V. Rostovtsev, M. S. Zubairy, and M. O. Scully, Optical imaging beyond the diffraction limit via dark states, Phys. Rev. A **78**, 013803 (2008).
[33] D.-S. Ding, Z.-Y. Zhou, B.-S. Shi, X.-B. Zou, and G.-C. Guo, Image transfer through two sequential four-wave mixing process in hot atomic vapor, Phys. Rev. A **85**, 053815 (2012).
[34] D.-S. Ding, J.-H. Wu, Z.-Y. Zhou, B.-S. Shi, X.-B. Zou, and G.-C. Guo, Multiple image storage and frequency conversion in a cold atomic ensemble, Phys. Rev. A **87**, 053830 (2013).
[35] M. Kiffner, J. Evers, and M. S. Zubairy, Resonant Interferometric Lithography Beyond the Diffraction Limit, Phys. Rev. Lett. **100**, 073602 (2008).